Dalton Transactions

ROYAL SOCIETY OF CHEMISTRY

PERSPECTIVE

View Article Online
View Journal | View Issue

Check for updates

Cite this: *Dalton Trans.*, 2024, **53**, 17110

Uranium extraction by metal–organic frameworks: advanced materials for new sorption possibilities

Mathéo Henry, Damien Rinsant, Jérome Maynadié and Michaël Carboni *

Received 2nd August 2024,
Accepted 24th September 2024

DOI: 10.1039/d4dt02208d

rsc.li/dalton

This review examines the advances and applications of metal–organic frameworks (MOFs) in the field of the extraction of uranium from various sources, focusing on their potential to address critical issues in nuclear fuel cycles. MOFs, characterized by their high surface area, tunable porosity, and chemical versatility, offer a promising alternative to traditional extraction methods. The review paper provides a comprehensive analysis of the synthesis strategies, functionalization techniques, and adsorption mechanisms of MOFs tailored for uranium capture. Furthermore, the review discusses the challenges and future directions in the field, emphasizing the need for scalable production, real-world application testing, and environmental impact assessment. This review aims to highlight the potential of MOFs to improve the sustainability and efficiency of uranium extraction processes.

Introduction

In the quest for sustainable energy and advanced technological applications, the efficient extraction and recovery of valuable resources such as uranium are of importance.[1] Indeed, uranium extraction is a vital process for the nuclear energy industry, providing fuel for reactors that generate electricity. Traditional extraction methods often pose environmental concerns and are inefficient, necessitating the exploration of novel approaches. In recent years, metal–organic frameworks (MOFs) have emerged as promising candidates to address these challenges. MOFs, composed of metal ions or clusters coordinated to organic linkers, exhibit remarkable structural diversity, high porosity, and tailorable chemical functionalities. These unique properties make MOFs as versatile platforms for adsorption, separation or purification processes.[2] However, the effectiveness of MOFs in uranium extraction depends on their stability under the harsh conditions encountered in leaching processes. To be viable for practical application, MOFs must maintain their structural integrity and adsorption capacity in the presence of high concentrations of acids, salts, and other contaminants.

This review aims to provide a comprehensive overview of recent advances in the use of MOFs for the extraction of uranium based on the fundamental principles of MOF design and synthesis, to elucidate the mechanisms underlying uranium sorption in MOFs, and to discuss the key factors influencing extraction efficiency. The current state-of-the-art MOF materials specifically tailored for uranium extraction will be presented, highlighting their structural features, adsorption

ICSM, CEA, Univ Montpellier, CNRS, ENSCM, Marcoule, France.
E-mail: michael.carboni@cea.fr

Mathéo Henry

Mathéo Henry has obtained a Master's degree at the University of Montpellier in 2023. This Master's degree focuses on separative chemistry, materials chemistry and processes in the field of nuclear chemistry. He is currently preparing a PhD on actinide precipitation in organic phase after extraction by the addition of an organic ligand.

Damien Rinsant

Dr Damien Rinsant has obtained a Master degree at the University of Lyon in 2016. After this, he has joined the French Alternative Energies and Atomic Energy Commission at the ICSM to prepared a PhD on the development of MOF-type functionalized hybrid materials for the selective extraction of uranium. He is now working at EDF as Treatment-recycling project manager in the nuclear field since 2020.

capacities and selectivity in different conditions (mainly from seawater where MOFs have been extensively used).[3,4] In addition, the review will examine the challenges and opportunities associated with scaling up MOF-based extraction processes for industrial applications, including optimisation strategies, stability concerns and cost effectiveness.

Through this review, we aim to highlight the potential of MOFs as advanced materials for sustainable resource recovery and provide insights into future research directions and practical implications in the fields of energy, environmental protection and materials science.

Uranium extraction with functionalized MOFs

Zn-MOFs. In 1999, Li *et al.*[5] introduced a novel MOF based on zinc clusters and terephthalic acid. This material exhibited the remarkable property of retaining crystallinity and porosity even when fully desolvated. However, the water stability of Zn-based MOFs is typically low, which limits their application in solution processes.[6] Few materials synthesised from zinc clusters have been investigated for uranium extraction.

In 2015, Wang *et al.*[7] developed a Zn-based material structured like Zn(HBTC)(L).$(H_2O)_2$ with L = (*N*4,*N*4′-di(pyridine-4-yl)biphenyl-4,4′-dicarboxamide) and HBTC = benzenetricarboxylic acid for uranyl uptake from seawater. This structure features hexagonal channels with an aperture of 4 Å, decorated with free-standing acylamide and carboxyl groups. Extraction tests involved a 10 mL batch of uranyl solution at 100 ppm in contact with 10 mg of material. At pH 2, the maximum adsorption was reached within five minutes, with SZ-3 exhibiting one of the fastest uranyl adsorption kinetics described in this review. The Langmuir isotherm model yielded a maximum sorption capacity of 115 mg g^{-1}. Uranium ions were desorbed using a solution of 0.1 M Na_2CO_3, with approximately 93% of the uranium recovered. Wang *et al.* further studied the adsorption, desorption, and stability of the Zn-based MOF in seawater, demonstrating an extraction efficiency of 0.53 mg g^{-1} after 1 minute of contact in 1 L of 6 ppb uranyl concentrated seawater. Subsequent extractions with the same material showed extraction efficiencies of 0.51 and 0.47 mg g^{-1}, respectively. PXRD analysis and IR revealing deprotonation of carboxylic acid and coordination with UO_2^{2+} and carbonyl of the acetylamide confirmed the regenerability of the MOF.

In 2016, Liu *et al.*[8] synthesised a new material called Zn(ADC)(4,4′-BPE)$_{0.5}$ for uranyl extraction. This material was synthesised with an equimolar ratio of $Zn(NO_3)_2$, 4,4′-BPE (*trans*-1,2-bis-4-pyridylethene), and ADC (azobenzene-4,4′-dicarboxylic acid) in DMF. The linker ADC contains azo groups expected to act as potential sorption sites for uranyl. Extraction tests involved a 10 mL batch of uranyl solution at 200 ppm in contact with 5 mg of material. The optimal conditions were determined to be 140 minutes of contact at pH = 6. IR analysis confirmed uranyl uptake onto the material, with a maximum uptake capacity of 337 mg g^{-1} calculated from the Langmuir isotherm. Thermodynamic parameters indicated an endothermic and spontaneous adsorption process, with a chemisorption mechanism proposed for uranyl adsorption.

Still, on Zn-based MOFs, Song *et al.*[9] developed materials bridged with functionalised isophthalic acid (hydrogen, hydroxy, amino, and nitro) for uranyl adsorption in water and seawater media. These four materials were synthesised with Zn$(NO_3)_2$, acylamide ligand (*N*4,*N*4′-di(pyridine-4-yl)biphenyl-4,4′-dicarboxamide), and functionalised isophthalic acid to give four materials named; 1-H, 1-OH, 1-NH_2, and 1-NO_2. The PXRD pattern of these MOFs exhibited few differences, suggesting a similar 3D framework for all four materials. CO_2 adsorption uptake revealed a higher pore volume for 1-NH_2 and 1-H compared to the other two MOFs, attributed to the organic units in the pore wall. The pH effect on the extraction process was investigated, demonstrating the influence of the functional group on the extraction efficiency (Fig. 1).

Jérome Maynadié

Dr Jérôme Maynadié received his Master degree at the University of Toulouse III and completed his PhD degree in coordination chemistry from the University of Toulouse. In 2005, he began to research on f-elements coordination chemistry at the French Alternative Energies and Atomic Energy Commission (Saclay). In 2007, he joined the team of Dr Bruno Chaudret to develop magnetic and luminescent nanoparticles. In 2009, he joined the University of Montpellier as assistant professor. His research interest is focused on coordination chemistry to design new molecular species or bulk architectures for photocatalysis and energy applications.

Michaël Carboni

Michaël Carboni received his Master's degree from the University of Orsay (Paris XI) and completed his Ph.D. in Inorganic Chemistry from the University of Grenoble. In 2012, he started a postdoc with Professor Wenbin Lin at the University of North Carolina and the University of Chicago to design porous materials for the extraction of Uranium from Seawater. In 2014, he joined the French Alternative Energies and Atomic Energy Commission as a permanent researcher in Marcoule. His research interest is focused on the development of metal–organic frameworks for energy and environmental purposes.

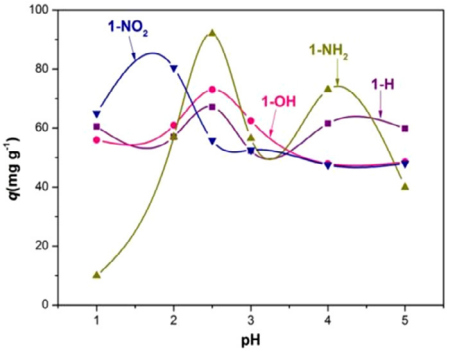

Fig. 1 Effect of pH on U(IV) sorption on Zn-based MOFs (ω = 5 mg, C_0 = 100 mg L^{-1}, t = 300 min, T = 25 °C and V = 10 mL). *J. Radioanal. Nucl. Chem.*, **310**, 317–327, © 2016.

The adsorption efficiency of uranyl on MOF 1-NO_2 and 1-NH_2 is strongly influenced by pH, with similar adsorption capacities achieved at pH 1.5 for one material and at pH 2.5 or pH 4 for the other. These properties render the MOF suitable for pH-dependent chemical processes. The contact time required to reach maximum adsorption was also investigated, with equilibrium achieved in less than 10 minutes for 1-NO_2 and 1-OH, but over 150 minutes for the other two materials. Calculated maximum adsorption capacities using the Langmuir isotherm model were significantly higher for 1-NO_2 (165 mg g^{-1}) than for the other materials, with 1-NH_2 slightly higher (95 mg g^{-1}) than 1-H (76 mg g^{-1}) and 1-OH (66 mg g^{-1}). However, uranium desorption was incomplete regardless of the eluent used for these materials. The conditions proposed by the authors resulted in only 11.3% uranium recovery for MOF 1-NO_2. Extraction tests in simulated seawater resulted in about 50% uranium recovery for 1-OH and 1-NH_2, but negligible recovery for the other two materials.

Zhang *et al.*[10] developed a new coumarin-modified material based on MOF-74, one of the more economical MOFs, with poor stability in aqueous media. Loaded with coumarin, this MOF exhibited high UV photosensitivity and potential for photo-switched (photodimerisation) uranium storage/release. The pore size of MOF-74 was controlled by the structure of the zinc cluster, enabling the successful synthesis of microporous–mesoporous MOF-74. Coumarin was then loaded inside in varying proportions, measured by elemental and thermogravimetric analysis, yielding several new materials. These were analysed by N_2 adsorption, CO_2 adsorption and PXRD.

The addition of coumarin inside MOF-74 ("A-2") slightly modified the PXRD pattern, and with increasing coumarin content, both micropores and mesopores were modified, resulting in narrower pore size distributions. UV irradiation of A-3: X wt% resulted in reduced N_2 uptake, suggesting a more compact phase inside the material due to photodimerization of coumarin. The thermostability of irradiated MOF remained unchanged for materials loaded with less than 28.2% coumarin.

However, for A-3: 28.2 wt% MOF, a loss of guest molecules at 114 °C was observed before irradiation, which decreased to 6.9% after irradiation, indicating guest retention due to photodimerisation. Uranyl uptake was performed with a 10 mL batch of uranyl solution in contact with 10 mg of material at pH 4 for 5 hours (Fig. 2). Kinetic studies indicated a chemisorption process, with U(VI) ions localised in a monolayer uniform adsorption. The influence of microporous–mesoporous synthesis on uranium uptake was evident between MOF A-1 and A-2, with the adsorption capacity enhanced by coumarin loading within the structure. However, as the coumarin content increased, the extraction efficiency decreased due to reduced pore accessibility for uranyl ions. A-3: 11.7 wt% exhibited high efficiency, with U(VI) adsorption unaffected by UV irradiation. Conversely, for A-3: 20.6 wt%, A-3: 28.2 wt%, and A-3: 35.7 wt%, the adsorption capacity decreased after UV irradiation, indicating the efficiency of the photo-switching behaviour towards U(VI) for materials loaded with more than 20.6% coumarin. Furthermore, the adsorption capacity could be restored after UV light irradiation at 250 nm wavelength, confirming the reversibility of photodimerisation. Uranyl desorption was more efficient with a 0.1 M HCl solution, eluting about 80% of U(VI) for A-3: 28.2 wt%. Re-irradiation of the MOF resulted in full recovery of the remaining 20% of uranyl.

Zr-MOFs. In 2008, researchers at the University of Oslo introduced novel materials synthesised by solvothermal methods using zirconium chloride and a carboxylic acid based linker.[11] These materials, known as the UiO series, composed of three different MOFs – UiO-66, UiO-67, and UiO-68 – each named according to the number of benzene rings in the linear linker based on carboxylic coordination functions: one, two, and three, respectively. The exceptional stability of these MOFs in aqueous environments stems from their high coordination level and robust binding between oxygen and zirconium. Consequently, the UiO family has been extensively investigated for metal extraction applications in both neutral and acidic aqueous conditions. UiO-68 boasts large tetrahedral apertures exceeding 10 Å, while the outstanding stability of UiO-66 remains unaltered regardless of the linker length. In 2013, Carboni *et al.*[12] improved the chemical structure of UiO-68 by incorporating a phosphorylurea derivative, as a bridging ligand, resulting in a functionalised material with potential

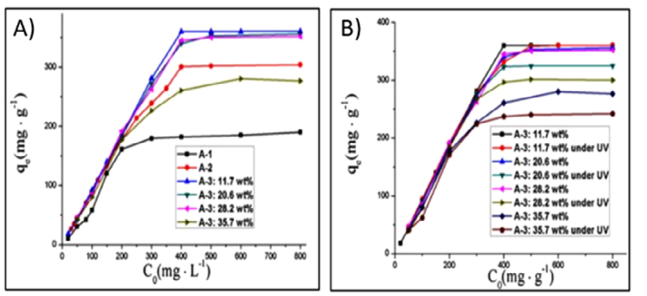

Fig. 2 Adsorption isotherms of uranium ion on Zn-MOF-74 (A) $m_{adosrbent}$ = 10 mg, pH = 4, t = 5 h and T = 298 K (B) under ambience or after UV (320 nm) irradiation. $m_{adsorbent}$ = 10 mg, pH = 4, t = 5 h and T = 298 K, $t_{irradiation}$ = 30 min. Reproduced with permission from Journal.

affinity for uranyl ions. Moreover, the phosphorylurea moiety offers the opportunity for post-functionalisation reactions, allowing the synthesis of dihydroxyphosphorylurea UiO-68 derivatives (Fig. 3).

The porosity of these materials was rigorously investigated by BET-C analysis and DFT calculations. A significant decrease in surface area, from 3730 $m^2\ g^{-1}$ to 750 $m^2\ g^{-1}$, was observed from MOF 1 to MOF 3, confirming internal functionalisation. However, the relative pore volume, as assessed by dye uptake measurements, was found to be greater for MOF 3 compared to MOF 2. Following extensive material characterisation, the group investigated the uranium extraction performance of these materials in both water and simulant seawater media. The extraction procedure involved a 10 mL batch of uranyl acetate solution (50–100 mg L^{-1}) in contact with 10 mg of adsorbent for one hour at pH = 2.5. MOF 2 exhibited a saturation sorption capacity (q_{max}) of 217 mg g^{-1} in water and 188 mg g^{-1} in seawater, while MOF 1 and 3 displayed lower efficiencies. Despite attempts, uranium desorption proved to be challenging, even with a 1 M HCl eluant. The coordination mode of uranyl with phosphorylurea was investigated by DFT calculations in the gas phase to work with a water-free uranyl complex, revealing a monodentate coordination with two protonated ligands and a slight preference for phosphoryl oxygen over carbonyl oxygen.

More recently, W. Wang *et al.*[13] have also used phosphorylurea to develop a new functionalized MOF. The material was synthesised by a solvothermal route (DUT-5 and DUT-6-NH_2) and then by *in situ* induced etching method (DUT-5-POR). This approach provided a scalable structure with enhanced hydrophilicity. The resulting BET surfaced was 1328 $m^2\ g^{-1}$ for DUT-5-POR, which is lower than the calculated 1860 $m^2\ g^{-1}$ for DUT-5. The authors explain this reduction by the presence of phosphorylurea group in the DUT-5 channels. Additionally, DUT-5-POR exhibited mesoporous pores, which increased the kinetics and adsorption capacity for uranyl ions in the MOF. The effect of pH on U(VI) adsorption was positive, with adsorption increasing as pH rose, reaching a maximum of 105 mg g^{-1}. This enhancement is due to the electrostatic and coordination interaction between phosphorylurea and uranyl ions.

In 2016, Luo *et al.*[14] explored the efficiency of UiO-66 and its amine derivative for U(VI) extraction. After thorough characterisation, UiO-66-NH_2 exhibited a lower surface area in BET analysis compared to UiO-66 (1050 *vs.* 1382 $m^2\ g^{-1}$). Optimal conditions for uranyl extraction were determined as 4 mg of sorbent for 10 mL of uranyl nitrate solution (5–120 ppm) at pH = 5.5 for 4 hours. The maximum sorption capacities calculated by Langmuir isotherm models were close for both materials, 109 and 114 mg g^{-1} for UiO-66 and UiO-66-NH_2, respectively. The introduction of the amino group led to a decrease in the surface area and pore volume of UiO-66, which may account for the similar adsorption efficiency of the two materials. The selectivity of UiO-66 and its amine derivative was evaluated by introducing competing ions during the sorption process, with no significant effect on uranyl uptake observed under the studied conditions.

Zirconium-based metal–organic frameworks (MOFs) are renowned for their exceptional stability, particularly in aqueous environments. However, their stability can be influenced by various factors, including pH. While zirconium MOFs generally exhibit excellent resistance to acidic conditions, their behavior in alkaline environments can vary. In general, these materials tend to maintain their structural integrity at lower pH values, but as the pH increases, the MOF framework may become susceptible to hydrolysis or ligand exchange. This can result in the breakdown of the crystalline structure and the leaching of zirconium ions into the solution. The specific pH threshold at which instability occurs can depend on the particular zirconium MOF and the nature of the organic linkers used in its construction. Therefore, understanding the pH-dependent stability of zirconium MOFs is crucial for their effective application in various fields, especially those involving aqueous environments.

The concentration of ions in solution is also a critical factor influencing the stability of MOFs beside the pH. In this way, a novel zirconium-based MOF functionalized with an amidophosphonate ligand was proposed and used in harsh sulfuric acid conditions ($[SO_4^{2-}]$ = 1 M, pH = 2), commonly encountered in uranium leaching processes.[15] This MOF, derived from the UiO-68-NH_2 precursor, was prepared using an efficient post-synthetic modification technique that achieved a high degree of functionalization (95%). The resulting material demonstrated remarkable stability and the MOF exhibited uranium extraction capabilities in this condition, adsorbing U up to 25 mg g^{-1}.

Another effective method to enhance adsorption performance is by introducing defects into the structure. These defects create open sites within the framework, facilitating the efficient adsorption of the desired elements. An additional advantage of creating defect in the framework is the ability to manipulate functional groups as well as pore sizes.[16] To achieve this degree of tailoring, several methods have been studied. X. Hou *et al.*[17] reviewed the current progress in induced defects in MOFs, covering both defect insertion strategies and their impacts. Regarding uranium adsorption using a MOF with defects, Z. Zhao *et al.*[18] report a defective Zr-based MOF with remarkable performance. The introduction of defects into the structure was achieved by the addition of

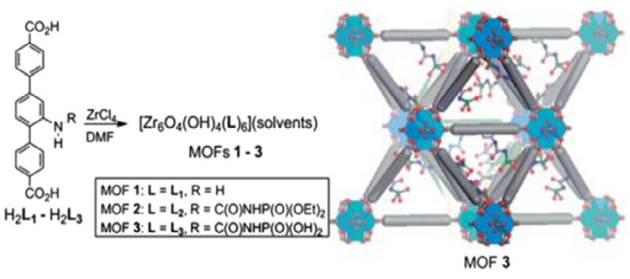

Fig. 3 Design of a UiO-68 type MOF for the U extraction from seawater. Reproduced from *Chem. Sci.*, 2013, **4**, 2396–2402 with permission from the Royal Society of Chemistry.

H_2BDC instead of the original organic linker (H_3BDC). This controlled addition was performed at different H_2BDC/H_3BDC molar ratios (1, 2, 3 and 4) leading to the defective M808-1, M808-2, M808-3 and M808-4 respectively. The optimal pH range for maximum adsorption efficiency is between pH 6 and 9 (Fig. 4A). Furthermore, the more defects present in the material, the higher the adsorption efficiency (Fig. 4B).

As previously discussed, improving the stability of a MOF often involves strengthening the metal-linker bond. In 2015, Mouchaham *et al.*[19] developed new materials based on trioxobenzene with greater stability in complexing media than UiO-67, and proposed zirconium phosphate MOF as a promising ultrastable MOF.

The pioneering study on lanthanide and actinide extraction using zirconium-phosphate materials was carried out by Luca *et al.*[20] Three phosphonic acid ligands, derived from benzene rings, were employed to synthesise MOFs with $ZrOCl_2$ clusters in aqueous media. Due to the strong affinity between the phosphonic acid ligand and the zirconium cluster, the synthesis often resulted in poorly crystalline or even amorphous materials, referred to as unconventional MOFs.[21] Consequently, this publication extensively investigates the synthesis of these new materials with the aim of obtaining samples with convincing BET surface areas and high crystallinity.

Recently, Zheng *et al.*[22] introduced a novel material for uranium extraction based on zirconium clusters and tetraphosphonate linkers. To overcome the problems associated with Zr phosphonate MOFs, which generally have poor crystallinity and a non-3D framework, they employed two steric linkers named TppmH8 (tetrakis[4-(dihydroxyphosphoryl)phenyl] methane) and TppaH8 (1,3,5,7-tetrakis(4-phosphonophenyl) adamantine). In addition, they pioneered an innovative synthesis method for gradual material formation by diffusion through ionothermal synthesis. Among the three synthesised materials, two exhibited interesting surface areas (225 $m^2\ g^{-1}$ for SZ-2 and 572 $m^2\ g^{-1}$ for SZ-3). In particular, SZ-3 showed exceptional stability over a pH range of 1 to 11, as well as resistance to concentrated nitric acid, hydrochloric acid, and aqua regia. Extraction tests were performed using 10 mg of material in contact with 10 mL of uranyl solution at a concentration of 10 mg L^{-1}. The pH range studied was 1 to 7, with particular emphasis on pH values of 1 and 4.5. Kinetic studies at pH 4.5 revealed rapid adsorption within 5 minutes for SZ-2 (72.3% of U extracted) and within 60 minutes for SZ-3 (80.2% of U extracted).

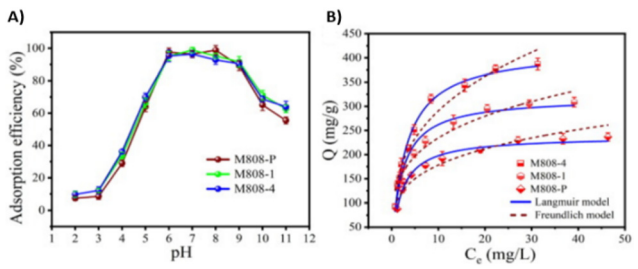

Fig. 4 (A) The effect of pH on uranium adsorption by MOF-808 containing defects. (B) Adsorption isotherms fitted by Langmuir and Freundlich isotherm model. Reproduced with permission from Journal.

Other MOFs. A subclass of MOF materials are zeolitic imidazolate frameworks (ZIFs), which exhibit zeolite or zeolite-like topologies, along with remarkable chemical robustness and thermal stability.[23] Among these, ZIF-8, synthesised from zinc salt and 2-methylimidazole as a linker, has been improved by encapsulating Fe_3O_4 nanoparticles for uranyl extraction.[24] The encapsulation of iron particles, of approximately 10 nm in size, inside the MOF resulted in a 26% reduction in surface area (from 1543 to 1137 $m^2\ g^{-1}$).

Furthermore, the stability of Fe_3O_4@ZIF-8 was evaluated, showing stability over the pH range of 1 to 6. Uranium extraction involved contacting a 4 mg batch of material with 10 mL of uranyl solution at 250 mg L^{-1}, followed by rapid removal of the MOF with a magnet. Kinetic studies revealed rapid adsorption within the first 30 minutes, reaching equilibrium in 2 hours. Maximum uranyl adsorption occurred at pH 3–4, with a measured maximum adsorption capacity of 523 mg g^{-1}.

Comparison with ZIF-8 and Fe_3O_4 particles showed the order of maximum adsorption capacity to be Fe_3O_4 < Fe_3O_4@ZIF-8 < ZIF-8, although specific values were not provided. Lanthanide separation from uranyl ions gave selectivity factors ranging from 56 for lanthanum to 132 for europium. However, uranyl desorption with a sodium carbonate solution at 1 mol L^{-1} achieved only 77% uranyl recovery.

In 2024, J. Guo *et al.*[25] investigated a new sulfur-decorated ZIF-68 synthesized *via* a solvothermal route for the removal of uranium from seawater. In addition to its ability to regenerate at low pH, SF@ZIF-68 exhibit a maximal removal efficiency of 79.02% and an efficiency capacity of 200.83 mg g^{-1} at pH 6. Furthermore, SF@ZIF-68 display a 66.61% capture efficiency and a distribution coefficient approaching 10^4 towards UO_2^{2+} even when vanadium ions are 3000 times more concentrated than uranium. The dodecahedron shape of the particle explains the efficient adhesion of sulphur groups, while the soft acid-hard base principles favour the affinity of sulphur group for UO_2^{2+} over hard proton ions.

In 2023, A. Das *et al.*[26] developed a malonitrile (MN) functionalized MIL-100(Fe). The synthesis of MIL-100(Fe) and its functionalization with MN have been previously documented in the literature.[27,28] The authors reported a removal efficiency of 97% and an adsorption capacity of 270 mg g^{-1} at 232 K and a pH of 10. The increase in adsorption capacity at higher pH is explained by the uranium speciation. Specifically, in solutions with a pH of 8–10, ($[(UO_2)(CO_3)_2]^{2-}$ and $[(UO_2)(CO_3)_3]^{4-}$) complexes were found. The coordination interactions between UO_2^{2+} and C≡N are significantly stronger for these complexes compared to those at lower pH levels. Additionally, MIL-100 (Fe)_MN maintained over 90% uranium adsorption efficiency after five adsorption/desorption cycles. Structural, morphological, and crystallographic analyses confirmed that the material's integrity was preserved throughout these cycles.

C. Bi *et al.*[29] studied a novel adsorbent (PCN-222-OM) for the recovery of U(VI) in wastewater. The pH of the system sig-

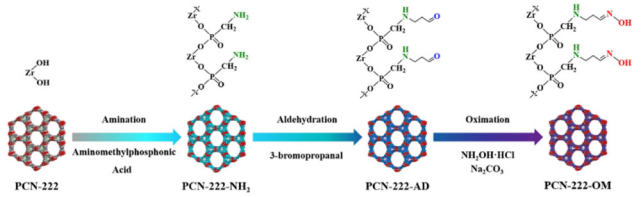

Fig. 5 Schematic diagram of synthetic procedures of PCN-222-OM. Reproduced with permission from Journal.

nificantly impacts the material's adsorption capacity for U(VI), with different functional groups exhibiting optimal pH ranges for adsorption. The authors compared the effect of pH on U(VI) adsorption by (PCN-222-OM) but also from its intermediaries (Fig. 5). The initial PCN-222 exhibited a maximum adsorption capacity at pH 4 equal to 361.4 mg g^{-1}, while the two intermediates (PCN-222-NH_2) and (PCN-222-AD) showed maximum adsorption capacities at pH 5 of 314.5 and 306.1 mg g^{-1} respectively. Finally, the studied material PCN-222-OM was found to be optimal at pH 6, with a maximum adsorption capacity of 403.4 mg g^{-1}.

Chromium MOFs have been developed for many years, notably at the Lavoisier Institute (France). In 2005, Férey *et al.*[30] introduced MIL-101, which is characterized by unusually large pore sizes (29–34 Å). Synthesised under hydrothermal conditions from chromium nitrate and H_2BDC, MIL-101 exhibits stability over months in air atmosphere and remains unaltered when treated with organic solvents. Its large pore apertures (12–16 Å) and pore size make it promising for large molecule adsorption.

Hence, Zhang *et al.*[31] investigated uranium extraction using MIL-101 derivatives, leveraging MIL-101's stability in acidic media and sufficiently large apertures for uranyl adsorption. They developed materials functionalised *via* a coordination-based post-synthetic modification (PSM) strategy. First, MIL-101 was heated and dried under vacuum to remove any water molecules coordinated on the Cr(III) centres. Subsequently, ethylenediamine (ED) was introduced to coordinate the coordinatively unsaturated chromium centres (CUS) of MIL-101. MIL-101 was modified with nitrogen-based linkers for its potential affinity for metal ions (particularly uranyl) due to the soft donor nature of nitrogen groups (Fig. 6).

The peak intensity exhibited a slight decrease after post-synthetic modification (PSM) and no modification of crystallinity was detected by PXRD analysis for ED-MIL-101. However, the amount of ethylenediamine (ED) grafted onto MIL-101 induced significant morphological changes on the material surface.

Zhang *et al.* controlled the amount of ethylenediamine introduced onto MIL-101, resulting in four samples labelled A, B, C, and D, with an Ed/Cr ratios of 0.34, 0.68, 0.98, and 1.42, respectively. N_2 adsorption revealed a significant reduction in surface area with an increasing amount of ED, attributable to the decrease in pore volume following the replacement of coordinated water by ethylenediamine.

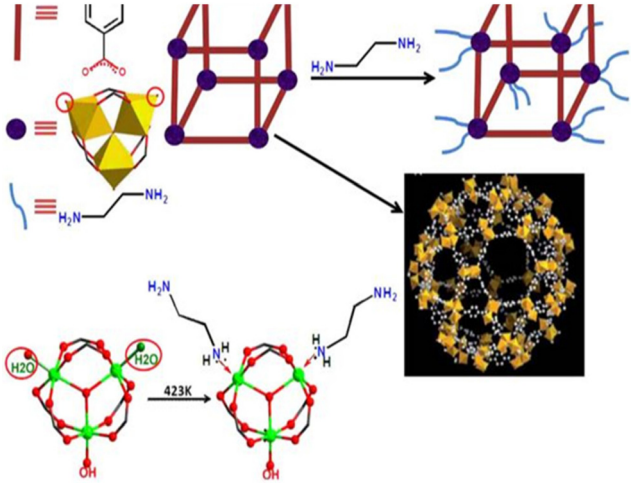

Fig. 6 Work road-map of the ED-functionalized MIL-101(Cr) through the post-synthetic modifications. Reprinted with permission from *Sci. Rep.*, **5**, 13514. © 2015 Nature.

Uranium extraction was investigated using batches of 100 mL of U(VI) solution at 100 ppm, with 50 mg of MOF at varying pH levels for 10 or 48 hours; however, Zhang *et al.* did not provide kinetic studies. pH optimisation resulted in complete uranyl extraction at pH 4.5 for 48 hours (Q_t = 200 mg g^{-1}). Moreover, the maximum extraction efficiency of ED grafted to MIL-101 was achieved with an Ed/Cr ratio of 0.68, with varying amounts of ED leading to decreased extraction efficiency. The diffusion of uranyl within functionalised MIL-101 proved to be more challenging with higher ED grafting on the chromium cluster. Unfortunately, ED-MIL-101 exhibited a 58% loss in uranyl extraction efficiency after 4 cycles of reusability due to the hydrolysis of the ED grafted to the chromium centres (back-extraction with an aqueous solution at pH < 2).

Similarly, Bai *et al.*[32] developed two new materials based on the post-functionalisation of coordinatively unsaturated chromium centres (CUS) with ethylenediamine and diethylenetriamine (DETA). These materials were compared with a MOF called MIL-101-NH_2, obtained through the nitration of terephthalic acid followed by reduction to yield the expected functionalised linker. Functionalisation was confirmed by PXRD, IR, and BET analysis, and thermal stability was attested by TGA analysis. Uranyl adsorption experiments were performed with uranyl nitrate solutions ranging from 5 to 200 ppm. *n* batch experiments, 10 mL of uranyl solutions were contacted with 10 mg of material, stirred for specified times at room temperature and controlled pH. The pH effect on U(VI) sorption was investigated over a pH range of 3 to 6. MIL-101 showed no pH effect, in contrast to the three other MOFs, which exhibited strong pH dependence. Although the maximum adsorption was achieved at pH 6, pH 5.5 was chosen for subsequent sorption studies to avoid uranyl hydrolysis and precipitation. Adsorption equilibrium was reached after 2 hours, with a rapid rate observed within the first

30 minutes for all MOFs. Functionalisation led to maximum adsorption capacities of 350, 200, and 90 for MIL-101-DETA, MIL-101-ED, and MIL-101-NH_2, respectively. Notably, no morphological changes were observed in MEB analysis, and only a slight decrease in peak intensity was noted in PXRD analysis after uranyl uptake.

Back-extraction of U(VI) was achieved at more than 99% for all materials with a solution at pH < 3. MIL-101-NH_2 demonstrated reusability, while the extraction efficiency of the other two materials decreased by 30% after U(VI) desorption, which was attributed to CUS hydrolysis during the extraction process, similar to ED-MIL-101(Cr) by Zhang *et al.*

Selectivity tests were performed for MIL-101-DETA, showing a strong pH-dependent adsorption efficiency and higher selectivity for competitive ions at pH 5.5 than at pH 4. The sorption mode of uranyl on the new materials was shown to be in good agreement with Langmuir isotherm models, suggesting a monolayer uniform adsorption of U(VI) for MIL-101-ED and MIL-101-DETA. Conversely, MIL-101-NH_2 did not fit well with either Langmuir or Freundlich models, probably due to a physisorption mechanism resulting from steric hindrance of the aromatic rings. EXAFS analysis of the loaded materials with U(VI) confirmed differences in sorption mechanisms between NH_2 and ED/DETA functionalised MOFs. Furthermore, FTIR analysis revealed no adsorption of nitrate ions as counterions on the MOF surface. Combined with EXAFS-derived distances, these results led to the identification of the uranyl complex $[UO_2][NH_2]_2O_2[H_2O]_3$ for MIL-101-ED and MIL-101-DETA. MIL-101 has opened up intriguing new avenues for functionalisation, leveraging unsaturated chromium centres to significantly enhance uranium extraction efficiency compared to linker functionalisation. However, Li *et al.* proposed an alternative functionalisation approach for MIL-101 using click chemistry on MIL-101-NH_2.[33] Initially synthesised from 2-aminoterephthalic acid, MIL-101-NH_2 was modified *via* a post-synthetic route to yield two additional materials (Fig. 7).

This approach offers a wide range of new materials owing to the facile functionalisation of the alkyne group, which also allows for the use of hard donors such as oxygen to increase the affinity for uranyl. The functionalisation of the material was monitored by IR spectroscopy, liquid ^1H NMR, and PXRD. Initially, the IR study unequivocally confirmed the formation of azide from MIL-101(CR)-NH_2, indicated by a peak at 2124 cm^{-1}. Subsequently, the disappearance of the same peak confirmed the transformation of azide group, but not necessarily the formation of triazole carboxylic acid. RMN after digestion also corroborated formation azide group and transformation. However, the formation of triazole cannot be definitively confirmed, although the product obtained exhibited a significant shift in aromatic peaks. Powder XRD patterns indicated poor crystallinity for all three materials. Li *et al.* attributed the broad Bragg reflection to the small particle size observed in TEM analysis. Nevertheless, comparison with the simulated pattern of MIL-101 confirmed the formation of chromium-based materials, with no significant modification in PXRD patterns observed after functionalisation. N_2 adsorption experiments revealed a decrease after each transformation, from 1907 for MIL-101(CR)-NH_2 to 890 $m^2\ g^{-1}$ for, suggesting framework distortion or pore obliteration of the materials. Uranium sorption was investigated using batches of 1 mL of uranyl nitrate solution contacted with 1 mg of adsorbent at various concentrations, pH levels, and contact times.

As expected, pH exerted a significant effect on uranium extraction for MIL-101(CR)-triazole-COOH. Relatively poor extraction efficiency was observed below pH 3 and above pH 11. However, maximum adsorption occurred at pH 5 to 10, probably due to protonation of the carboxylic acid below this range, and the influence of uranyl species in solution within this pH range on extraction efficiency. Subsequently, extraction tests were carried out at pH 7 to avoid uranyl ion precipitation. Kinetic adsorption showed a rapid rate within 30 minutes, reaching equilibrium at around 2 hours, consistent with the study of Bai *et al.* on MIL-101-DETA. Similar to MIL-101-DETA, a pseudo-second-order rate model agreed well with the adsorption isotherm of MIL-101(CR)-triazole-COOH, suggesting chemical chelation rather than physical adsorption in the uranium sorption process. A maximum adsorption capacity of 304 mg g^{-1} was measured, with an estimated value of 314 mg g^{-1} from the Langmuir model. This q_m is very similar to that of MIL-101-DETA mentioned earlier, and it's noteworthy that the N_2 adsorption for this material is close to that of MIL-101 (CR)-triazole-COOH (1074 *vs.* 890 $m^2\ g^{-1}$).

The selectivity of MIL-101(CR)-triazole-COOH for uranyl over rare earths and transition metals is presented in Table 1. MIL-101(Cr)-triazole-COOH exhibits higher selectivity for U(VI) over transition metals such as cobalt or nickel compared to lanthanides. Nevertheless, MIL-101(CR)-triazole-COOH demonstrates considerable potential for uranyl uptake (Kd approximately 18 000 mL g^{-1}) and remarkable selectivity for U(VI) over competing ions. Additionally, successful uranyl desorption was achieved using a 1 M Na_2CO_3 solution (98% uranium recovery). Interestingly, a lower uranium recovery rate was observed with a 1 M HNO_3 solution (85% uranium recovery), in contrast to the acidic elution method (pH < 3) used by Bai *et al.* and Zhang *et al.* Unfortunately, the regeneration efficiency of MIL-101(CR)-triazole-COOH decreased by 50% after three cycles. Uranyl uptake in seawater exhibited lower adsorption efficiency than in water (75%). Molecular dynamics studies elucidated the mechanisms of uranyl ion adsorption. Simulation revealed complete uranyl extraction by MIL-101

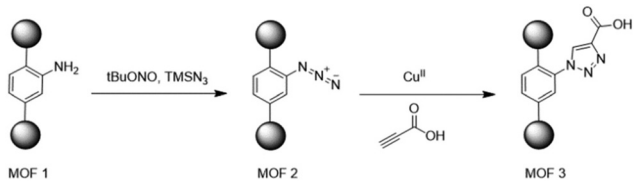

Fig. 7 Post-synthetic strategy based on amino-derived MIL-101 for the effective extraction of uranium(VI). Reproduced with permission from Journal.

Table 1 Selectivity of MIL-101(CR)-triazole-COOH for uranyl over rare earth and transition metals. Reprinted with permission from *ACS Appl. Mater. Interfaces*, **8**(45), 31032–31041. © 2016 American Chemical Society

	Co^{2+}	Ni^{2+}	Zn^{2+}	Sr^{2+}	La^{3+}	Ce^{3+}	Sm^{3+}	Gd^{3+}	Yb^{3+}
$S_{U/M}$	8530.1	115.2	37.1	2828.1	8.0	19.3	5.5	10.2	16.1

(CR)-triazole-COOH within 5 ns, with no subsequent modifications observed after 10 ns. Most of the uranyl ions migrated to the MOF/solution interface, with only a small fraction entering the MOF structure, in contrast to MIL-101(CR)-NH_2 where approximately one third of the uranyl ions remained in solution. Protonation of the carboxyl groups reduced the binding capacity of MIL-101(Cr)-triazole-COOH, consistent with the uranium extraction process. Density profiles of uranyl ions over different simulation times corroborated these results. Carboxyl groups on MIL-101(CR)-triazole-COOH showed intense binding with uranyl ions, with an average distance of 2.24 Å between oxygen atoms and uranyl ions and five coordinated oxygen atoms in the first coordination shell.

Using Density Functional Theory analysis, Li *et al.* proposed the formation of three pentacoordinate complexes of triazole carboxylic acid with uranyl ions. The most energetically favourable binding mode involved uranyl coordination in a monodentate fashion with one carbonyl oxygen atom and four water molecules. Li *et al.* demonstrated the efficacy of linker post-functionalisation for chromium-based materials, achieving extraction values comparable to those of MOFs post-functionalised on CUS, but offering a wider range of binding motifs to explore. In 2016, De Decker *et al.*[34] synthesized a new material based on MIL-101, termed CMPO@MIL-101, in three steps as show in Fig. 8.

The functionalisation percentage for CMPO@MIL-101 was determined to be 0.5 mmol of CMPO per gram of MIL101. In an initial study by De Decker *et al.*, the adsorption of europium and the extraction selectivity towards zinc and yttrium were investigated. Batches containing 50 mg of MOF were exposed to 50 mL of europium solution at various concentrations. Only one pH value was studied, and equilibrium was reached within 5 hours. The maximum adsorption, determined using a Lagergren pseudo-first order kinetics model, was found to be 10 mg g^{-1}. The selectivity between europium and other elements was calculated as SFEu/Y = 3.2 and SFEu/Zn = 8.5. In 2017, the same CMPO@MIL-101 material was tested for uranyl adsorption.[35] Its affinity for uranyl ions compared to various rare earth metals was evaluated. In this investigation, batches containing 10 mg of CMPO@MIL-101 were exposed to 5 mL of elemental solutions at concentrations of 10 or 500 μg L^{-1} for 30 minutes at pH 4. Remarkably, De Decker reported that the material reached uranyl adsorption equilibrium in less than 10 minutes, indicating its suitability for use in adsorption column setups. Furthermore, CMPO@MIL-101 exhibited no activity for uranium adsorption at pH values below 4. Selectivity tests revealed a favourable selectivity towards rare earth elements (SF > 30), but significant thorium adsorption occurred alongside uranyl (SF ≈ 1.3).

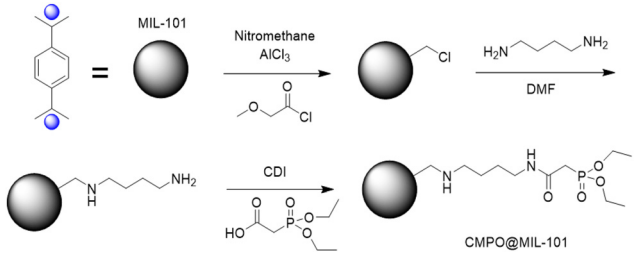

Fig. 8 Step-wise anchoring of CMPO on MIL-101(Cr). Mil-101: pristine MOF, –Cl: chloromethylated, –NH_2: aminated, MIL-101-LIG: completed CMPO on MIL-101. Reproduced with permission from Journal.

In a column cartridge test, 10 mg of sorbent was loaded and conditioned to the appropriate pH with nitric acid. Then, 15 mL of uranyl solution at 100 mg L^{-1} was passed through the column at a flow rate of 1 mL min^{-1} for the adsorption test. Uranyl desorption was performed with 15 mL of ammonium oxalate solution at pH 4. The column felt testing for 5 adsorption/desorption cycles, with full recovery of uranyl observed each time. De Decker *et al.* estimated a 15 wt% loss of ligand after the 5 adsorption/desorption cycles. Chui *et al.*[36] produced a remarkably porous material called HKUST-1, crafted from copper and trimesic acid. This coordination polymer, originating in the 20th century, boasts substantial pores of about 1 nm in diameter and offers the prospect of chemical functionalisation.

The Hong Kong University team elucidated that HKUST-1 is composed of octahedral secondary building units, with a dicopper(II) tetracarboxylate building block at each vertex.

In 2013, Feng *et al.*[37] marked the debut of HKUST-1 in uranyl adsorption. This copper-based MOF was used in its pristine state without any functionalisation. The purity and crystallinity of HKUST-1 were validated by PXRD analysis. Using the BJH method, the average mesopore diameter was estimated to be around 13.5 nm, a significant improvement over the original HKUST-1 described by Chui *et al.* For the uranyl adsorption tests, batches of 50 mL of uranyl solution at 200 ppm were contacted with 50 mg of HKUST-1 for a duration of 2 hours under controlled pH conditions. The pH effect was investigated, revealing that over 99% of uranyl was recovered within a pH range of 2–8, with optimal conditions identified at pH 6. This preference stemmed from the increasing negative charge of the material with increasing pH, while uranyl complexes remained positively charged at near neutral conditions. Equilibrium adsorption was assessed at three temperatures, with values ranging from 744 mg g^{-1} to 810 mg g^{-1} as the temperature increased from 298 to 318 K. The adsorption iso-

therm closely followed the Langmuir model, suggesting surface adsorption of uranyl on the material.

In the kinetic sorption study, equilibrium was reached within 60 minutes, fitting well with a pseudo-second-order kinetic model. Interestingly, temperature variation did not significantly alter the adsorption isotherm or affect the equilibrium adsorption capacity at low initial uranyl concentrations. The adsorption mechanism was further investigated using IR spectroscopy, particularly focusing on the oxygen band of the linker. Feng *et al.* proposed that partial negative charges localised on the carboxyl group could interact with uranyl ions. Thus, the adsorption properties of HKUST-1 at pH 6 were attributed not only to coordination but also to electrostatic Coulomb interactions.

The high affinity of the Cu^{2+} sites for water facilitated greater dispersion in aqueous media, thereby increasing the accessibility to the MOF for uranyl ions. However, the subsequent desorption of uranyl ions from the MOF proved to be unsuccessful. The water stability of HKUST-1 was reported to be very low. Hence, in 2015, Zhang *et al.* developed a new water-stable material based on HKUST-1 for the adsorption of uranyl from low-concentration wastewater.[38] They used polyoxometalate (POM) materials as templating agents to enhance water stability, resulting in the preparation of HKUST-1@$H_3PW_{12}O_{40}$ (MOFs@POMs). The synthesis process followed the typical HKUST-1 procedure, with the addition of $H_3PW_{12}O_{40}$ in a Cu/W ratio of 1. Interestingly, this material exhibited a pore diameter of 0.95 nm, in contrast to the 13.5 nm pore diameters reported by Feng *et al.* for HKUST-1. Adsorption tests were carried out using batches of 100 mL of low concentration (1 mg L^{-1}) uranyl solution with 20 mg of adsorbent at room temperature for 4 hours. Maximum adsorption occurred at pH 6, with equilibrium reached after 2 hours, during which 80% of the uranyl ions was adsorbed within 30 minutes. The selectivity of HKUST-1@$H_3PW_{12}O_{40}$ was assessed by testing against interfering ions individually compared to uranyl. No reduction in uranyl uptake was observed, although the amount of adsorbed ions was not specified. However, the selectivity of HKUST-1@$H_3PW_{12}O_{40}$ was not specifically evaluated in this study.

Uranyl desorption from the MOF resulted in 98% recovery with a 0.1 M Na_2CO_3 solution. The adsorption efficiency of HKUST-1@$H_3PW_{12}O_{40}$ decreased from 0.9760 mg g^{-1} in the first test to 0.9040 mg g^{-1} in the third test. PXRD analysis confirmed that the crystallinity of the material remained unchanged after successive adsorptions, although SEM analysis showed an increasingly rough surface area with further adsorption. FT-IR patterns before and after adsorption clearly demonstrated uranyl interaction with POM and carboxylic acid of HKUST-1, confirming the regenerability of the material. The adsorption isotherm was fitted to Langmuir and Freundlich models, with the Langmuir model showing better fit and a calculated maximum adsorption capacity of 14.58 mg g^{-1}. Additionally, the pseudo-second-order model fit well, suggesting that a chemical adsorption mechanism governed the process.

In 2013, Yang *et al.*[39] investigated the adsorption of uranyl on MOF-76. MOF-76, composed of lanthanide ions and BTC, was first studied for its photoluminescence when dispersed in uranyl solution. A significant decrease in luminescence intensity was observed with increasing uranyl concentration. This phenomenon was related to the reduced energy transfer from BTC to Tb^{3+} ions upon adsorption of uranyl ions on MOF-76. The sorption properties of MOF-76 were then investigated using Y-MOF-76, which is characterised by a low framework density.

The stability of the yttrium-based material was confirmed by PXRD, which showed stability within a pH range of 2.5–3, although partial collapse was observed at pH 2.

Evaluation of uranyl adsorption over the pH range of 2 to 6 revealed a maximum adsorption efficiency of 300 mg g^{-1}. Notably, the adsorption efficiency declined steeply beyond pH 3, contrary to the typical uranyl uptake behaviour in MOFs. Equilibrium adsorption was achieved within 5 hours for a uranyl solution with a concentration of 140 mg L^{-1}.

The maximum adsorption capacity of 300 mg g^{-1} was in good agreement with values obtained from the Langmuir isotherm model. Selectivity analysis demonstrated superior uranyl selectivity over competing ions at pH 2.5 compared to pH 3. While selectivity towards Pb^{2+}, Zn^{2+}, and Cs^{+} ions was modest, it was remarkably strong for Ni^{2+}, Co^{2+}, and Cr^{3+}. Uranyl recovery exceeded 90% using a 0.1 M Na_2CO_3 solution.

Currently, there's only one documented case of uranyl adsorption by anionic exchange in the literature. Li *et al.*[40] investigated the U(VI) extraction capability of Co-SLUG-35. This material consists of positive fragments $[Co(H_2O)_4(4\text{-}4'\text{-bipy})_2]^{2+}$ (bipy = 4,4′-bipyridine) and negative 1,2-ethanedisulfonate ions (EDS^{2-}). Structurally, it forms cationic layers composed of six-coordinated cobalt, with two bipyridine ligands and four water molecules. The cobalt clusters are interconnected *via* π stacking with two bipyridine ligands, while each cationic layer is linked by free EDS^{2-} and water molecules. Adsorption tests involved batches of 10 mL of uranyl solution in contact with 10 mg of Co-SLUG-35. Uranyl adsorption on Co-SLUG-35 exhibited a strong pH dependence, even in anionic exchange extraction. Notably, adsorption efficiency peaked at pH 9 within a pH range of 1–10, where the uranyl structure in solution, calculated to be $[UO_2(CO_3)_3]^{2-}$, facilitated anionic exchange with EDS^{2-}. Kinetic evaluation revealed that equilibrium was reached after four hours, with the pseudo-second-order model fitting well, indicating chemical interaction-driven adsorption. The maximum adsorption capacity was quantified at 118 mg g^{-1}, consistent with the Langmuir model prediction of 119 mg g^{-1}.

Uranyl desorption using an $EDSNa_2$ solution achieved only 67% efficiency. After the first reusability test, the extraction efficiency of Co-SLUG-35 dropped to 61 mg g^{-1}, but remained constant in subsequent tests. The adsorption mechanism was elucidated by the disappearance of characteristic EDS^{2-} bands and the appearance of carbonate bands in IR analysis. In addition, PXRD patterns and EDS analysis confirmed the substitution of EDS by uranyl.

Actinides MOFs

Actinides can also be considered as nodes in the structure of the MOFs. The versatility of actinide oxidation states makes them ideal candidates for achieving new MOF coordination modes. Although the literature is less abundant, some examples can be given. Metal–organic frameworks based on terephthalate linkers have been the most studied over the decades. Uranium and thorium remain the most studied actinide elements due to their low activity and radiotoxicity. Falaise *et al.*[41] studied the solvothermal synthesis of thorium with H_2BDC using DMF/H_2O. Three structures were obtained depending on the use of DMF and/or H_2O. The first structure ($Th(BDC)_2(DMF)_2$) is obtained by using DMF; it involves the coordination of thorium to eight oxygen atoms coming from different terephthalate linkers and two from DMF (Fig. 9A).

The second structure ($Th(BDC)_2$) involves the use of H_2O in the solvothermal synthesis.

Here, the thorium is coordinated to eight oxygens coming from different terephthalate linkers (Fig. 9B). Finally, the last one ($Th_6O_4(OH)_4(H_2O)_6(BDC)_{6.6}DMF_{12}H_2O$) was obtained using DMF and H_2O and coordinates the thorium with three types of oxygen atoms (Fig. 9C).

Uranium–organic frameworks based on terephthalate have also been investigated. Falaise *et al.*[42] synthesised these materials by solvothermal methods using DMF and/or DMF and H_2O. Two different symmetries of $U_2Cl_2(BDC)_3(DMF)_4$ were obtained (triclinic $P\bar{1}$ and monoclinic $C2/c$) (Fig. 10). In both cases, the uranium has the same coordination environment. In fact, there is one chlorine atom and eight oxygen atoms are involved. Six come from the terephthalate and two from the *N*,*N*-dimethylformamide.

These structures imply the formation of different networks. Chelating terephthalate linkers are responsible for the 3D structuring of the material, whether the structure is triclinic or monoclinic. Of the three terephthalate molecules coordinated to uranium, two are involved in the formation of the 2D planar network, while the third is responsible for the formation of the 3D structure (Fig. 11). The difference between the two networks is due to the orientation of the benzene rings. In fact, in the triclinic structure, the benzene rings are all face in the same direction, whereas in the monoclinic structure they alternate between one direction and the other.

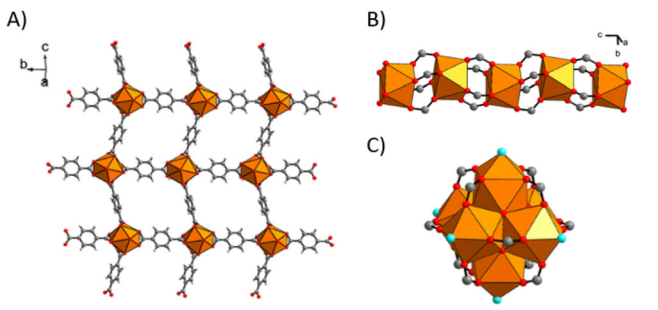

Fig. 9 Thorium–organic frameworks based BDC structures synthesized with (A) DMF: $Th(BDC)_2(DMF)_2$ (B) H_2O: $Th(BDC)_2$ (C) DMF and H_2O: $Th_6O_4(OH)_4(H_2O)_6(BDC)_6{\cdot}6DMF.12H_2O$. Reprinted with permission from *Inorg. Chem.*, 2015, **54**(5), 2235–2242. © 2015 American Chemical Society.

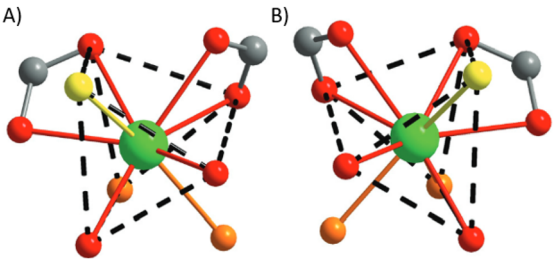

Fig. 10 Uranium–organic frameworks based BDC coordination modes of the different structures (A) triclinic $P\bar{1}$ (B) monoclinic, $C2/c$. Green: uranium; red: carboxyl oxygen; orange: formamide oxygen; yellow: chlorine; grey: carbon. *Dalton Trans.*, **44**, 2639–2649, © 2015.

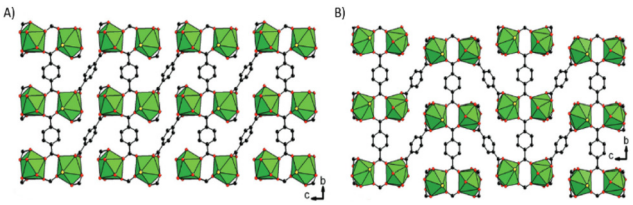

Fig. 11 Connection modes of (A) triclinic (B) monoclinic $U_2Cl_2(BDC)_3(DMF)_4$. *Dalton Trans.*, **44**, 2639–2649, © 2015.

Other organic linkers have been investigated, Mishra *et al.*[43] reported a rare uranium–organic framework with diamidoximyl as the organic linker. Here, the tautomeric flexibility of benzene-1,4-diamidoxime (1,4-(DAO)Bz) (Fig. 12) provides a three-dimensional non-interpenetrated MOF with a triclinic $P\bar{1}$ space group.

This U-MOF was prepared by an aqueous route leading to the formation of $[(UO_2)_4(O)_2(C_8H_8N_4O_2)(C_8H_{10}N_4O_2)_3(H_2O)_2]{\cdot}Cl{\cdot}nH_2O$ (Fig. 13). Three coordination modes of 1,4-(DAO)Bz can be observed: unidentate dianions (red), μ_2-zwitterion (yellow) and unidentate and μ_2-zwitterionic (blue).

As the affinity of phosphonates for the uranyl cation is well known, their use as an organic linkers for the synthesis of MOFs is of interest. Chen *et al.*[44] reported two U-MOF synthesised under mild solvo/hydrothermal conditions. Compound **1** $K_8[N(C_2H_5)_4]_2(UO_2)_{17}(H_2O)_4[CH_2(PO_3)_2]_8[CH_2(PO_3)(PO_3H)]_4{\cdot}16H_2O$ (Fig. 14A) and compound **2** $[N(C_2H_5)_4]_4(H_2O)_2(UO_2)_{10}$

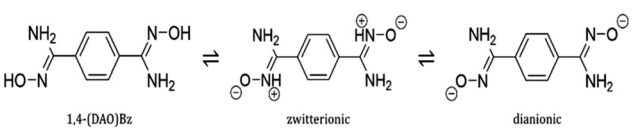

Fig. 12 Molecular structures of the different forms of benzene-1,4-diamidoxime. Reprinted (adapted) with permission from *Cryst. Growth Des.*, 2019, **10**, 5466–5470. © 2019 American Chemical Society.

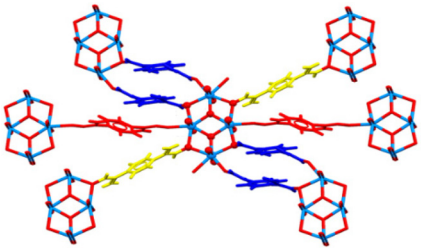

Fig. 13 Uranium–organic frameworks based 1,4-(DAO)Bz coordination environment. Reprinted (adapted) with permission from *Cryst. Growth Des.*, 2019, **10**, 5466–5470. © 2019 American Chemical Society.

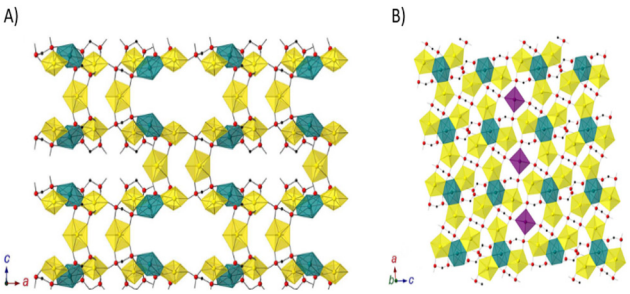

Fig. 14 Uranium–organic frameworks based phosphonate organic linker structures (A) solvothermal (B) hydrothermal. Reproduced with permission from *Chin. J. Chem.*, **39**(3), 597–604 © 2021. Chinese Chemical Society.

$[CH_2(PO_3)_2]_5[CH_2(PO_3)(PO_3H)]_2{\cdot}10H_2O$ (Fig. 14B) were obtained respectively.

Three uranium coordination environments were found. In both U-MOF structures: hexagonal bipyramid, pentagonal bipyramid and tetragonal bipyramid. Depending on the type of synthesis (hydro or solvothermal), the structural arrangement between the three different uranium centres changes. While compound **1** exhibits a centrosymmetric phase at room temperature, a single crystal to single crystal transformation was found by lowering the temperature. The chiral phase obtained at a lower temperature has a better photoluminescence intensity than the centrosymmetric phase.

Outlook: uranium extraction by MOFs precipitation

We have seen the possibility of extracting U by linker functionalisation of the MOFs and also the possibility of forming MOFs based on U. The combination of these two approaches can lead to a new strategy for extracting metals from solution by precipitating the metals as valuable MOF material. In this strategy, the binding agent of the MOF is then the precipitating agent and the materials obtained can be used directly (as in gas separation, catalysis, *etc.*) or converted, in particular into oxides.

This novel concept has already been proposed for the recycling of Li-ion batteries through an open-loop process,[45] which aims to reduce the volume of waste while producing valuable materials, in particular metal–organic frameworks (MOFs), in large quantities. The process starts by dissolving nickel, manganese and cobalt (NMC) batteries in acidic solutions (such as HCl, HNO_3, or H_2SO_4/H_2O_2). After the addition of organic components and heat treatment, different MOFs are formed. The resulting solutions are analysed using inductively coupled plasma, and the materials are characterised by powder X-ray diffraction, N_2 adsorption, thermogravimetric analysis, and scanning electron microscopy. Using benzene tricarboxylic acid as a ligand, selective formation of an aluminium-based MOF, known as MIL-96, is achieved, which is noted for its gas storage properties. The supernatant is reused to precipitate additional metals as MOFs by introducing a second set of ligands. Depending on the conditions, these subsequent MOFs are either copper-based (HKUST-1) or nickel–manganese-based with a novel crystalline structure. This method shows promising results at the laboratory scale, converting 15 grams of waste into 10 grams of MOFs, and offers significant potential for scaled-up MOF production.

To extract U under different conditions, an adaptation of this strategy may be of interest in the future. The fact to possibly form MOFs with the precipitating agent (linker) and the metal can help to selectively isolate the metal from a complex solution. In addition, the metal can then be stored (if toxic by example) as a MOFs or can be recovered after hydrolysis of the MOF. The fact that MOFs can be easily converted to oxides is also of interest to the nuclear industry, whose process is based on the use of UOx or MOx fuel. As waste is a major issue in the nuclear fuel cycle (particularly in terms of societal acceptance), the development of such an approach could make it possible to reduce the amount of liquid effluent by reducing the number of steps in the spent fuel reprocessing process.

Finally, the use of biosourced precipitating agents could be considered as a way of moving towards increasingly environmentally responsible processes.

Conclusions

Recent research on modifying MOFs for uranium and lanthanide extraction has produced a number of effective materials with improved performance. The incorporation of functional groups into the framework of MOFs combines the advantages of MOFs (such as high porosity) with the strong affinity of the functional groups for uranium ions. Despite significant progress over the past decade, the use of functional group-decorated MOF materials for uranium extraction remains experimental and several challenges remain to be overcome. It is important to note that MOF materials are highly sensitive to external environmental conditions, including temperature, pH, and organic solvents. In particular, alkaline conditions can lead to the collapse of MOF structures. Due to the complexity of practical conditions, enhanced stability is essential for the successful application of MOF materials in real-world scenarios.

We have also seen the possibility of forming MOFs with U and that it is also possible to extract metals from solution as a

MOFs material (with 3d metals). We believe that such a strategy may be of interest and should be developed in the future for the extraction of U under different conditions (depending of the application).

Author contributions

HM, DR, JM, MC: writing – review & editing.

Data availability

No primary research results, software or code have been included and no new data were generated or analysed as part of this review.

Conflicts of interest

There are no conflicts to declare.

Acknowledgements

We thank the French Alternative Energies and Atomic Energy Commission (CEA) for financial support (PRATA).

References

1 D. K. Singh, S. Mondal and J. K. Chakravartty, *Solvent Extr. Ion Exch.*, 2016, **34**, 201–225.
2 Y. Song, B. Deng, K. Wang, Y. Zhang, J. Gao and X. Cheng, *J. Environ. Chem. Eng.*, 2024, **12**, 113967.
3 C. W. Abney, R. T. Mayes, T. Saito and S. Dai, *Chem. Rev.*, 2017, **117**, 13935–14013.
4 Y. Xie, Z. Liu, Y. Geng, H. Li, N. Wang, Y. Song, X. Wang, J. Chen, J. Wang, S. Ma and G. Ye, *Chem. Soc. Rev.*, 2023, **52**, 97–162.
5 H. Li, M. Eddaoudi, M. O'Keeffe and O. M. Yaghi, *Nature*, 1999, **402**, 276–279.
6 N. C. Burtch, H. Jasuja and K. S. Walton, *Chem. Rev.*, 2014, **114**, 10575–10612.
7 L. L. Wang, F. Luo, L. L. Dang, J. Q. Li, X. L. Wu, S. J. Liu and M. B. Luo, *J. Mater. Chem. A*, 2015, **3**, 13724–13730.
8 S. Liu, M. Luo, J. Li, F. Luo, L. Ke and J. Ma, *J. Radioanal. Nucl. Chem.*, 2016, **310**, 353–362.
9 L. L. Song, C. Chen, F. Luo, S. Y. Huang, L. L. Wang and N. Zhang, *J. Radioanal. Nucl. Chem.*, 2016, **310**, 317–327.
10 L. Zhang, L. L. Wang, L. L. Gong, X. F. Feng, M. B. Luo and F. Luo, *J. Hazard. Mater.*, 2016, **311**, 30–36.
11 J. H. Cavka, S. Jakobsen, U. Olsbye, N. Guillou, C. Lamberti, S. Bordiga and K. P. Lillerud, *J. Am. Chem. Soc.*, 2008, **130**, 13850–13851.
12 M. Carboni, C. W. Abney, S. Liu and W. Lin, *Chem. Sci.*, 2013, **4**, 2396.
13 W. Wang, S. Ni, Y. Liu, Y. Zhao, Y. Meng and L. Yang, *Sep. Purif. Technol.*, 2024, **346**, 127409.
14 B.-C. Luo, L.-Y. Yuan, Z.-F. Chai, W.-Q. Shi and Q. Tang, *J. Radioanal. Nucl. Chem.*, 2016, **307**, 269–276.
15 D. Rinsant, E. Andreiadis, M. Carboni and D. Meyer, *Mater. Lett.*, 2019, **253**, 285–288.
16 S. Daliran, A. R. Oveisi, C.-W. Kung, U. Sen, A. Dhakshinamoorthy, C.-H. Chuang, M. Khajeh, M. Erkartal and J. T. Hupp, *Chem. Soc. Rev.*, 2024, **53**, 6244–6294.
17 X. Hou, J. Wang, B. Mousavi, N. Klomkliang and S. Chaemchuen, *Dalton Trans.*, 2022, **51**, 8133–8159.
18 Z. Zhao, R. Lei, Y. Zhang, T. Cai and B. Han, *J. Mol. Liq.*, 2022, **367**, 120514.
19 G. Mouchaham, B. Abeykoon, M. Giménez-Marqués, S. Navalon, A. Santiago-Portillo, M. Affram, N. Guillou, C. Martineau, H. Garcia, A. Fateeva and T. Devic, *Chem. Commun.*, 2017, **53**, 7661–7664.
20 V. Luca, J. J. Tejada, D. Vega, G. Arrachart and C. Rey, *Inorg. Chem.*, 2016, **55**, 7928–7943.
21 K. J. Gagnon, H. P. Perry and A. Clearfield, *Chem. Rev.*, 2012, **112**, 1034–1054.
22 T. Zheng, Z. Yang, D. Gui, Z. Liu, X. Wang, X. Dai, S. Liu, L. Zhang, Y. Gao, L. Chen, D. Sheng, Y. Wang, J. Diwu, J. Wang, R. Zhou, Z. Chai, T. E. Albrecht-Schmitt and S. Wang, *Nat. Commun.*, 2017, **8**, 15369.
23 M. Jian, B. Liu, G. Zhang, R. Liu and X. Zhang, *Colloids Surf., A*, 2015, **465**, 67–76.
24 X. Min, W. Yang, Y.-F. Hui, C.-Y. Gao, S. Dang and Z.-M. Sun, *Chem. Commun.*, 2017, **53**, 4199–4202.
25 J. Guo, Y. Li, C. Fu, C. Liu and M. Lei, *J. Solid State Chem.*, 2024, **336**, 124766.
26 A. Das, D. Roy, K. Erukula and S. De, *Chemosphere*, 2024, **348**, 140780.
27 K. Guesh, C. A. D. Caiuby, Á. Mayoral, M. Díaz-García, I. Díaz and M. Sanchez-Sanchez, *Cryst. Growth Des.*, 2017, **17**, 1806–1813.
28 H. Li, X. Feng, Y. Guo, D. Chen, R. Li, X. Ren, X. Jiang, Y. Dong and B. Wang, *Sci. Rep.*, 2014, **4**, 4366.
29 C. Bi, C. Zhang, C. Wang, L. Zhu, R. Zhu, L. Liu, Y. Wang, F. Ma and H. Dong, *Environ. Sci. Pollut. Res.*, 2024, **31**, 16554–16570.
30 G. Férey, C. Mellot-Draznieks, C. Serre, F. Millange, J. Dutour, S. Surblé and I. Margiolaki, *Science*, 2005, **309**, 2040–2042.
31 J.-Y. Zhang, N. Zhang, L. Zhang, Y. Fang, W. Deng, M. Yu, Z. Wang, L. Li, X. Liu and J. Li, *Sci. Rep.*, 2015, **5**, 13514.
32 Z.-Q. Bai, L.-Y. Yuan, L. Zhu, Z.-R. Liu, S.-Q. Chu, L.-R. Zheng, J. Zhang, Z.-F. Chai and W.-Q. Shi, *J. Mater. Chem. A*, 2015, **3**, 525–534.
33 L. Li, W. Ma, S. Shen, H. Huang, Y. Bai and H. Liu, *ACS Appl. Mater. Interfaces*, 2016, **8**, 31032–31041.
34 J. de Decker, J. de Clercq, P. Vermeir and P. van der Voort, *J. Mater. Sci.*, 2016, **51**, 5019–5026.
35 J. De Decker, J. Rochette, J. De Clercq, J. Florek and P. Van Der Voort, *Anal. Chem.*, 2017, **89**, 5678–5682.

36 S. S.-Y. Chui, S. M.-F. Lo, J. P. H. Charmant, A. G. Orpen and I. D. Williams, *Science*, 1999, **283**, 1148–1150.
37 Y. Feng, H. Jiang, S. Li, J. Wang, X. Jing, Y. Wang and M. Chen, *Colloids Surf., A*, 2013, **431**, 87–92.
38 H. Zhang, J. Xue, N. Hu, J. Sun, D. Ding, Y. Wang and L. Li, *J. Radioanal. Nucl. Chem.*, 2016, **308**, 865–875.
39 W. Yang, Z.-Q. Bai, W.-Q. Shi, L.-Y. Yuan, T. Tian, Z.-F. Chai, H. Wang and Z.-M. Sun, *Chem. Commun.*, 2013, **49**, 10415–10417.
40 J. Q. Li, L. L. Gong, X. F. Feng, L. Zhang, H. Q. Wu, C. S. Yan, Y. Y. Xiong, H. Y. Gao and F. Luo, *Chem. Eng. J.*, 2017, **316**, 154–159.
41 C. Falaise, J.-S. Charles, C. Volkringer and T. Loiseau, *Inorg. Chem.*, 2015, **54**, 2235–2242.
42 C. Falaise, A. Assen, I. Mihalcea, C. Volkringer, A. Mesbah, N. Dacheux and T. Loiseau, *Dalton Trans.*, 2015, **44**, 2639–2649.
43 M. K. Mishra, Y. P. Patil, S. P. Kelley and R. D. Rogers, *Cryst. Growth Des.*, 2019, **19**, 5466–5470.
44 L. Chen, Y. Zhang, Z. Weng, Z. Liu, J. Zhang, Y. Wang and S. Wang, *Chin. J. Chem.*, 2021, **39**, 597–604.
45 M. Cognet, J. Condomines, J. Cambedouzou, S. Madhavi, M. Carboni and D. Meyer, *J. Hazard. Mater.*, 2020, **385**, 121603.